Available online at www.sciencedirect.com
ScienceDirect
Journal of the European Ceramic Society 28 (2008) 2151–2159
www.elsevier.com/locate/jeurceramsoc

Microstructural self-healing effect of hydrothermal crystallization on bonding strength and failure mechanism of hydroxyapatite coatings

Chung-Wei Yang, Truan-Sheng Lui *

Department of Materials Science and Engineering, Frontier Material and Micro/Nano Science and Technology Center, National Cheng Kung University, No. 1 University Road, Tainan 701, Taiwan, ROC

Received 10 November 2007; received in revised form 14 February 2008; accepted 29 February 2008
Available online 1 May 2008

Abstract

Hydroxyapatite coatings (HACs) are synthesized on Ti–6Al–4V substrates using the plasma spraying process followed by autoclaving hydrothermal treatment at 125 and 150 °C. The quantitative analysis of X-ray diffraction indicates that the hydrothermal treatment is available to promote HA crystallization and further eliminate the amorphous and impurity phases of the HACs. The microstructural self-healing effect of hydrothermally treated HA coatings (HT-HACs) can be recognized as a nucleation and grain growth of nano-crystalline HA which tends to diminish the spraying defects through the hydrothermal crystallization. The significant hydroxy ion (OH^-) peak in XPS spectra detected from HT-HAC specimens represents that the hydroxyl-deficient state of plasma-sprayed HACs is significantly improved with the abundant replenished OH^- groups during the hydrothermal treatment. XPS analysis also demonstrates that the hydrothermal crystallization helps to promote the interfacial Ti–OH chemical reaction. The bonding strength of HA coatings is significantly improved from 32.4 MPa for the as-sprayed HACs to 38.9 MPa after 150 °C hydrothermal treatment. Through the statistical analysis of Weibull distribution function, the strengthening HT-HACs are generally reliable materials with a wear-out failure model. The failure morphologies of HT-HACs represent homogeneity with a larger area fraction of cohesive failure and a decreased adhesive failure area. The phenomena were resulted from the microstructural self-healing effect and the enhanced interfacial adhesion of HT-HACs to Ti–6Al–4V substrate.

Keywords: Hydroxyapatite; XPS; Mechanical properties; Failure analysis; Biomedical applications

1. Introduction

Hydroxyapatite ($Ca_{10}(PO_4)_6(OH)_2$, HA) is widely preferred as the biomaterial of choice in both dentistry and orthopaedics due to its favorable osteoconductive and bioactive properties.[1,2] *In vivo*, HA can bond physicochemically with bone and promote bone growth onto its surface.[3,4] Compared with other deposition methods, HA coatings (HACs) deposited using plasma spraying on metallic substrate exhibits enhanced interfacial strength and represents propensity of avoiding the inherent mechanical property limitations of HA without significant loss in biocompatibility.[5,6] However, during the high enthalpy of plasma spraying process, impurity phases ($Ca_3(PO_4)_2$, $Ca_4P_2O_9$, CaO, oxyhydroxyapatite, etc.) and amorphous calcium phosphate are generally identified in the sprayed HACs. These impurity and amorphous calcium phosphate have higher dissolution rate than crystalline HA in aqueous solutions, and it has a problem with decreasing the structural homogeneity, and the mechanical properties[7] for long-term clinical applications of HACs.

In order to improve the dissolution behavior, the microstructure and bonding degradation resulted from the undesirable amorphous and impurity calcium phosphate, some previous studies pointed out that the coating quality can be acquired by controlling the feedstock HA and the spraying parameters.[8–10] Furthermore, appropriate post-heat treatment was also an effective method to promote HA crystallization and improve the coating strength. Past reports have studied the changes of phase composition, crystallinity and microstructural feature of plasma-sprayed HACs after post-heat treatments.[11–15] It was recognized that an enhanced bonding strength could be achieved with the crystallization of HACs as a result of performing 500–600 °C post vacuum or atmospheric heat treatments.[16–18] However, the

* Corresponding author. Tel.: +886 6 2757575x62931; fax: +886 6 2380698.
E-mail addresses: Rei@mse.ncku.edu.tw (C.-W. Yang), z7408020@email.ncku.edu.tw (T.-S. Lui).

0955-2219/$ – see front matter © 2008 Elsevier Ltd. All rights reserved.
doi:10.1016/j.jeurceramsoc.2008.02.015

lack of heating temperatures over 600 °C for further improving the bonding strength was attributable to the formation of detrimental crystallization-induced cracks with high-temperature heat treatments.[17,18] It was difficult to simultaneously acquire high crystallinity and bonding strength without microstructural deterioration of HACs.

In our recent work, the hydrothermal treatment was more favorable for improving the HACs with a dense microstructure, a high crystallinity and low contents of impurity and amorphous calcium phosphate than the other heating method.[19] Thus, the aim of this present study is further to clarify the improved bonding strength correlated with the microstructural homogeneity through the self-healing effect of the hydrothermal crystallization. Furthermore, the reliability and the failure mechanism of as-sprayed and hydrothermally treated HACs will be examined by the statistical analysis of the Weibull model with the observation of failure morphologies.

2. Materials and methods

2.1. Atmospheric plasma spraying and hydrothermal treatment

Commercial high purity HA powder (XPT-D-701, Sulzer Metco) with particle size ranging from 15 to 40 μm was used in the coating process, and Ti–6Al–4V alloy (ASTM F-136 ELI) was selected as a substrate. Prior to spraying, substrates were grit-blasted with SiC grit, and the surface roughness (Ra) of substrates was controlled at about 6.0 ± 0.5 μm ($n = 10$). The HA powder was carried by high purity argon gas to the plasma torch with a power of 40.2 kW following the spraying parameters listed in Table 1, and the thickness of the HACs was controlled at a range of 120 ± 10 μm.

The hydrothermal treatment (HT) of plasma-sprayed HACs was performed at 125 °C, held for 6 and 12 h (HT125-6h, HT125-12h), and 150 °C, held for 6 h (HT150-6h) in an autoclave (Parr 4621, Pressure Vessel). The temperature deviation of hydrothermal treatment is about ±5 °C. Deionized water was used as the source of steam atmosphere in the autoclave during hydrothermal treatment, and the saturated steam pressures were 0.23 and 0.48 MPa at 125 and 150 °C, respectively.

2.2. Microstructural characterization of the HACs

The phase composition of the as-sprayed and hydrothermally treated HACs was identified by X-ray diffractometry (Rigaku D/MAX III. V), using Cu Kα radiation at 30 kV, 20 mA with a scan speed of 1° (2θ)/min. To evaluate the crystallinity, we adopted a commonly used index of crystallinity (IOC) defined from the ratio of three strongest HA peaks ((2 1 1), (1 1 2), and (3 0 0)) intensity of the HACs (Ic) and the HA powder (Ip) according to the relationship IOC = (Ic/Ip) × 100%.[9] This method assumes that the IOC of the as-received HA powder is 100%.

The surface morphologies of the as-sprayed and heat-treated HACs were examined by a scanning electron microscope (FE-SEM, Philips XL-40 FEG). For observation of the cross-sectional microstructure, the mounted specimens were carefully ground and polished to avoid inducing extra pores and cracks. The polished specimens were coated with carbon, and then examined by a backscattering electron image (BEI) of a SEM. Spraying defects content (in volume %), including microcracks and pores within the entire cross-sectional area of HACs, were defined and quantitatively calculated by an image analyzer (OPTIMAS 6.0).

Table 1
Plasma spraying parameters employed for preparing HACs[a]

Spraying parameter	Measurements
Primary gas (Ar), flow rate (L/min)	41
Secondary gas (H_2), flow rate (L/min)	8
Power (kW)	40.2
Powder feed rate (g/min)	20
Surface speed (cm/min)	8000
Stand-off distance (cm)	7.5

[a] Plasma-spraying was performed with Plasma-Technik system.

2.3. X-ray photoelectron spectroscopy (XPS)

The XPS analysis was performed in a VG Scientific ESCALAB 210 XPS system, using a standard Al Kα radiation source ($h\nu = 1486.6$ eV) at 15 kV with a power of 300 W. The base pressure of the XPS operating system was about 5×10^{-9} Torr. As required, the measured binding energy (BE) scale was referenced to the adventitious C 1s at the BE of 284.8 eV. For each specimen, survey spectra (from 0 to 1100 eV) and high-resolution spectra of the C 1s, Ca 2p, P 2p, O 1s and Ti 2p regions were obtained. The Gaussian peak-fitting routine was used in the analysis of high-resolution spectra for separating species in different chemical states.

2.4. Young's modulus and bonding strength measurements

According to the previous study,[20] we adopted a standard three-point bending test to evaluate the Young's modulus of plasma-sprayed HACs by Eq. (1).

$$E = \frac{PL^3}{4wt^3\delta} \quad (1)$$

E (GPa) is the Young's modulus, P (Newton, N) is the load, L (mm) is the span between supports, w (mm) is the specimen width, t (mm) is the specimen thickness, and δ (mm) is the specimen deflection at mid-span. For the Young's modulus measurements, the coating layer about 1.2-mm thick was coated on the substrate. After coating, the HAC test pieces with dimensions of 50 (l) mm × 5 (w) mm × 1 (t) mm were carefully cut from the substrates by a low-speed diamond saw along the coating/substrate interface, and then the substrate-removed HACs were hydrothermally treated at the above-mentioned conditions. Each as-sprayed and hydrothermally treated HAC test piece with an average surface roughness (Ra) of 2.6 ± 0.5 μm ($n = 10$) was given for the bending test. The bending crosshead speed was 0.01 mm/s, and the loading direction was perpendicular to the spraying deposition surface.

The bonding strength of the HACs was measured using a tensile adhesion test according to ASTM C633-01. Ti–6Al–4V cylindrical rods with dimensions of 25.4 mm (ϕ) and 50 mm (l) were used as substrates for the tests. Each test specimen was an assembly composed of a substrate fixture, to which the HACs of 120 ± 10 μm were applied, and a loading fixture. The loading fixtures were also grit-blasted and attached to the surface of the HACs using adhesive glue with an adhesive strength of about 60 MPa. After curing, the assemblies were subjected to tensile tests at a crosshead speed of 1 mm/min until failure. For the statistical significance of following Weibull analysis, twenty test specimens ($n = 20$) were performed for bonding strength measurements.

3. Results

3.1. Microstructural feature of hydrothermally crystallized HACs

Fig. 1 shows the X-ray diffraction patterns of the hydrothermally treated HACs. It is worth noting that the impurity phases, including $Ca_3(PO_4)_2$ (TCP), $Ca_4P_2O_9$ (TP) and CaO, are significantly eliminated after hydrothermal treatment. The sharpening of three strongest HA main peaks ($2\theta = 31.8°$, 32.2°, 32.9°, JCPDS 9-432) represents that the plasma-sprayed HACs further crystallized by autoclaving hydrothermal treatment at low heating temperatures. The quantitative results of the coating crystallinity (IOC, %) are listed in Table 2. Since the hydroxyl groups (OH^-) promote the reconstitution of amorphous calcium phosphate into crystalline hydroxyapatite,[21] therefore, the saturated steam pressure atmosphere of autoclaving hydrothermal treatment can effectively improve HA crystallization and eliminate the amorphous component of plasma-sprayed HACs with the replenishment of hydroxyl groups.

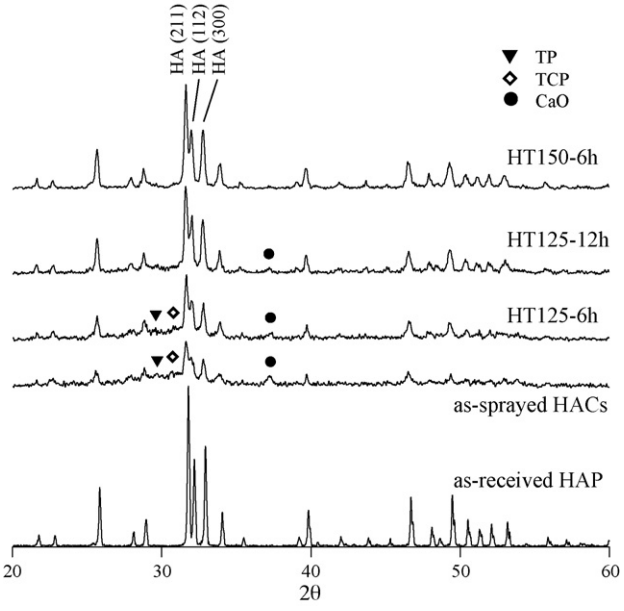

Fig. 1. The X-ray diffraction pattern of as-sprayed and hydrothermally treated HACs with various heating conditions. It reveals that the crystallinity and phase purity of HACs increase with hydrothermal treatment.

Table 2
Characteristics of as-sprayed and hydrothermally treated HACs

	Crystallinity (IOC, %)	Spraying defects (volume %)[a]	Young's modulus (GPa)[b]
HACs	20.3	3.9 ± 0.4	23.3 ± 0.8
HT125-6h	40.5	3.3 ± 0.3	30.9 ± 1.2
HT125-12h	59.6	2.7 ± 0.3	32.6 ± 1.1
HT150-6h	66.1	2.6 ± 0.2	33.2 ± 0.8

[a] Values were given as mean ± S.D., and each value was the average of ten tests ($n = 10$).
[b] Each value was the average of five tests ($n = 5$).

Fig. 2(a) shows the typical surface morphology of the plasma-sprayed HACs. It displays an accumulated molten splats feature with a fair amount of pores and thermal-induced microcracks during the rapid cooling stage. As indicated by arrows in Fig. 2(b) and (c), it is worth noting that evident nano-scale crystalline, which can be recognized as crystalline HA, is observed on the coating surface and in the vicinity of microcracks by 125 °C hydrothermal treatment. The surface crystalline further grain growth with increasing hydrothermal heating time, and the microcracks at the coating HT125-12h tend to be diminished as shown in Fig. 2(c). Considering the heat-treated HACs at a higher temperature 150 °C, the new-growth crystalline with a larger crystal size can also be found within microcracks as indicated by the arrow in Fig. 2(d).

The cross-sectional feature of the as-sprayed and hydrothermally treated HACs is shown in Fig. 3. Although the plasma-sprayed coatings possess inevitable spraying defects, including pores and thermal-induced microcracks, but they can be subjected to high densification due to the unapparent lamellar structure. Table 2 lists the quantitative analysis of the defects content. Generally, the hydrothermally treated HACs possess significant lower defects content (about 2.6%) and display a dense microstructure than the as-sprayed specimens (about 3.9%) as shown in Fig. 3(b)–(d). Considering the above microstructural observation by SEM, the grain growth phenomenon of heat-treated HACs induces the reduction of coating defects can be recognized as the self-healing effect by the hydrothermal treatment.

3.2. Young's modulus and bonding strength of the HACs

The Young's modulus of coatings obtained from the three-point bending test for the as-sprayed and hydrothermally treated HACs are shown in Table 2. The Young's modulus increased with increasing the HA crystallinity and decreasing the coating defect content. Table 3 shows the average bonding strength, measured by the tensile adhesion test, of the as-sprayed and various hydrothermally treated HACs. From the results of mechanical properties tests, it should be worth noting that both of the Young's modulus and the bonding strength of the plasma-sprayed HACs are significantly improved after the hydrothermal treatment. Considering the SEM observation shown in Figs. 2 and 3, it can be recognized that the improve-

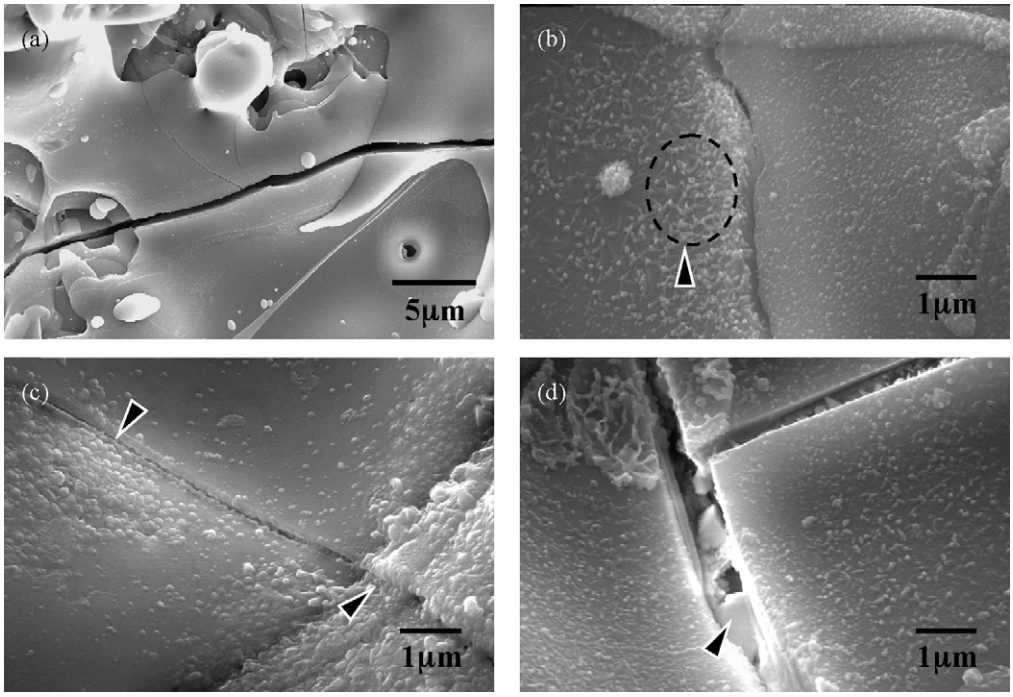

Fig. 2. Surface morphologies of (a) as-sprayed HACs, (b) HT125-6h, (c) HT125-12h, and (d) HT150-6h hydrothermally treated HACs.

ment of the HACs is resulted from the self-healing effect of hydrothermal crystallization.

3.3. Statistical evaluation of failure probability by the Weibull model

The Weibull distribution function,[22] which is a widely used statistical analysis method, was applied to evaluate the bonding strength fluctuation and failures of the HACs. Eq. (2) shows the general form of the Weibull distribution function.

$$F(\sigma_i) = \int_{\sigma=0}^{\sigma=\sigma_i} f(\sigma)\,\mathrm{d}\sigma = 1 - \exp\left[-\left(\frac{\sigma_i - \sigma_o}{\eta}\right)^m\right] \quad (2)$$

In Eq. (2), σ represents the bonding strength in this study, the parameter m represents the Weibull modulus (or called the shape parameter), η is the characteristics strength (or called the scale parameter) and σ_o is the minimum strength. Fitting the bonding strength data into the Weibull distribution function, the

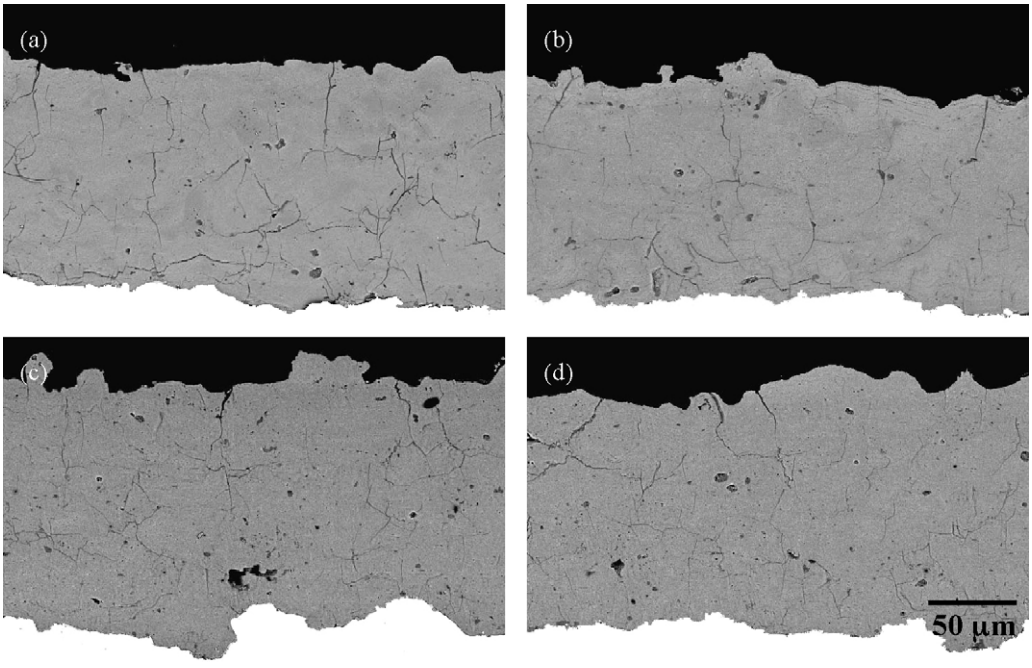

Fig. 3. Cross-sectional feature of (a) as-sprayed HACs, (b) HT125-6h, (c) HT125-12h, and (d) HT150-6h hydrothermally treated HACs.

Table 3
Results of the bonding strength measurements and the Weibull parameters of as-sprayed and hydrothermally treated HACs

	Bonding strength (MPa), σ[a]	Minimum strength (MPa), σ_o[b]	Characteristics strength (MPa), η[b]	Weibull modulus, m[b]
As-sprayed HACs	32.4 ± 1.5	26.8	33.1	3.8
HT125-6h	35.7 ± 0.9	31.7	36.1	4.9
HT125-12h	38.1 ± 1.2	32.6	38.7	5.0
HT150-6h	38.9 ± 1.0	33.3	39.4	6.4

[a] Each value was the average of twenty tests ($n = 20$).
[b] Data were calculated from $\ln\ln(1/1 - F(\sigma_i))$ vs. $\ln(\sigma_i - \sigma_o)$ plots (Fig. 4) using Eq. (4).

failure probability density function $f(\sigma)$ curves of the as-sprayed HACs for various hydrothermally treated samples are plotted in Fig. 4(a). The cumulative failure probability $F(\sigma_i)$ is estimated using the Benard's median rank (Eq. (3)),[23] which is a very close approximated solution of a statistical function,[23,24] and the reliability function $R(\sigma_i)$ with a relation of $R(\sigma_i) = 1 - F(\sigma_i)$ is defined as the survival probability[25] of the specimens herein.

$$F(\sigma_i) = \frac{i - 0.3}{n + 0.4} \tag{3}$$

Fig. 4(b) shows the natural logarithmic (ln) graphs for the cumulative failure probability at each corresponding bonding strength σ_i ($i = 1$–20) of the HACs, so as to graphically evaluate the Weibull modulus (m) from the slope of a least squares fitting method of Eq. (4), and the results of Weibull statistical analysis are listed in Table 3.

$$\ln\ln\left(\frac{1}{1 - F(\sigma_i)}\right) = m\ \ln(\sigma_i - \sigma_o) - m\ \ln\eta \tag{4}$$

According to the definition of Eq. (2), the failure behavior of materials is determined by three parameters m, η and σ_o. The Weibull modulus, which controls the shape of function curves, is a measure of the variability of the data. The characteristics strength η corresponds to the strength at which the cumulative failure is 63.2%. The minimum strength σ_o means that the failure probability of HACs lower than this strength is zero. The detail of Weibull statistical analysis on the failures and the effect of hydrothermal crystallization on the mechanical properties of the HACs will be discussed in the next chapter.

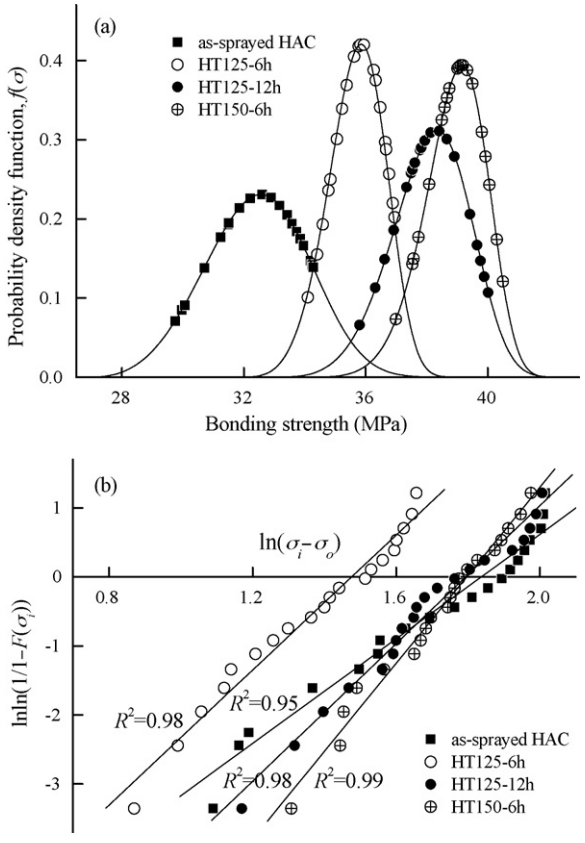

Fig. 4. (a) The failure probability density function $f(\sigma)$ curves, and (b) the Weibull distribution plots of the as-sprayed and hydrothermally treated HACs. $F(\sigma_i)$ is the cumulative failure probability at the corresponding bonding strength (σ_i) and the slope represents the Weibull modulus (m), which calculated by the least squares fitting method of Eq. (4) at a maximum coefficient of determination (R^2).

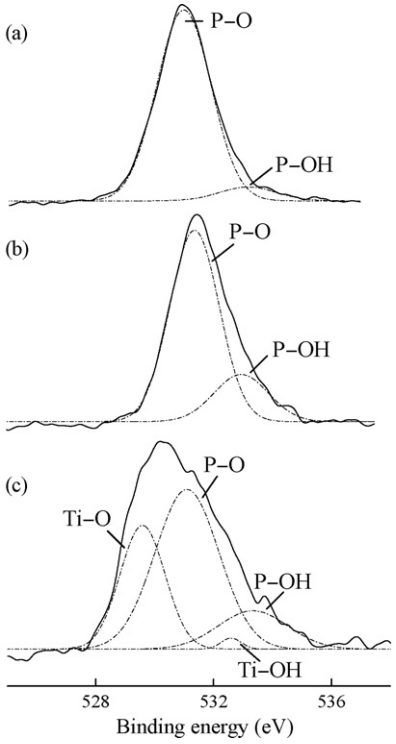

Fig. 5. XPS O 1s spectra curve-fitting results of (a) as-sprayed HACs, (b) hydrothermally treated (HT) HACs, and (c) the surface close to the HT-HAC/Ti–substrate interface.

4. Discussion

4.1. Self-healing effect of the hydrothermal crystallization

From the band observation of PO_4^{3-} and OH^- by FT-IR,[19,26,27] it provided the information concerning structural features such as the hydroxylation of HACs. In addition, the XPS analysis can further clarify the replenishment of hydroxyl groups (OH^-) and the reduction of the dehydroxylation state of hydroxyl-deficient HACs during the hydrothermal treatment in this study. Fig. 5 shows the high-resolution XPS O 1s spectra of the HACs, and the BE results after curve-fitting are listed in Table 4. The O 1s spectra presented in Fig. 5(a) and (b) consists two components at about BE = 531.4 eV and BE = 533.1 eV, which correspond to the P–O (PO_4^{3-}) and P–OH bonds of HA.[28–30] The relatively large integration area of the OH^- peak at hydrothermally treated (HT) HAC specimens with high degree of crystallinity shown in Fig. 5(b) can be recognized that the hydroxyl-deficient microstructure of plasma-sprayed HACs is significantly improved with the abundant replenished OH^- groups by hydrothermal treatment.

In Fig. 5(c), the O 1s spectra obtained from the HT-HAC/Ti–substrate interface are fitted with four peaks: the above-mentioned P–O, P–OH peaks of HA, the Ti–O peak at 529.6 eV and the Ti–OH peak at 532.5 eV. The Ti–O peak can be attributed to the surface oxide ion of Ti–substrate, and the peak at ΔBE about 3.0 eV from Ti–O peak can be assigned to the chemisorbed hydroxyl groups of Ti–OH.[29–31] Considering the rapid solidification of molten HA droplets during plasma spraying induces the formation of amorphous calcium phosphate at the HAC/Ti–substrate interface, the analysis results represent that the hydrothermal treatment promotes the interfacial crystallization through the chemical bonding of hydroxyl groups. The *in vitro* biocompatibility tests demonstrated that crystalline HA has a considerably lower dissolution rate and the presence of Ti–OH bonding can further enhance the bioactive properties of the HA coating by promoting the osteointegration process.[30,32] In our resent study, the HT-HACs showed a statistically higher extent of new bone apposition than the as-sprayed HACs,[33] and it could further achieve the initial fixation of implants in clinical use.

Fig. 6 shows a linear relationship between the Young's modulus and the crystallinity (IOC) of HACs. Since the Young's modulus is a measure of the inter-atomic binding forces, it is reasonable to suggest that the Young's modulus of HACs depends on the extent of crystallization.[18] Besides, the microstructural features such as porosity, lamellar structure and the contact between splats boundaries should be also considered as other influencing factors on the Young's modulus of a coating.[34,35] Therefore, the obvious improvement of the Young's modulus for HT-HAC specimens compared with the crystallized coatings in our previous study[18] can be recognized due to the self-healing effect of hydrothermal crystallization, and it will further enhance the fracture toughness of a coating.[9]

Table 4
Binding energy values of XPS O 1s spectra for the HACs

Samples	Binding energy of O 1s spectra (BE, eV)			
	Ti–O	P–O	Ti–OH	P–OH
As-sprayed HAC	–	531.2	–	533.4
HT-HAC[a]	–	531.4	–	533.1
HT-HAC/Ti interface	529.6	531.2	532.5	533.2

[a] HT-HAC: hydrothermally treated HA coating.

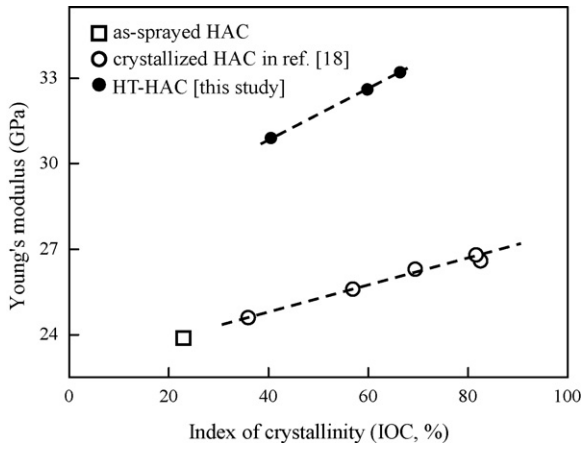

Fig. 6. A linear correlation between the Young's modulus and the crystallinity (IOC) of the HACs.

The evidences can be observed from the fracture specimens of HT-HAC test pieces after three-point bending tests. Fig. 7(a) represents a significant reduction of pores and cracks within

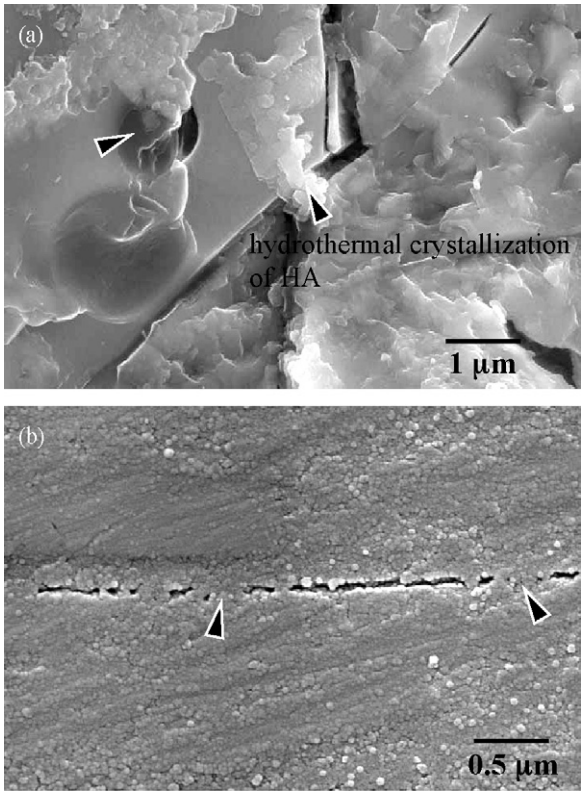

Fig. 7. The self-healing effect of hydrothermal crystallization (as indicated by arrows) on plasma-sprayed HACs observed at (a) the coating fracture surface after three-point bending test, and (b) the lamellar boundaries of the coatings.

coatings, and the lamellar boundaries are healed with the crystalline as indicated by arrows in Fig. 7(b). The microstructural homogeneity and the contact between splats boundaries are significantly improved after hydrothermal treatment. Thus, besides the nano-scale HA crystalline observed on the coating surface (Fig. 2), the hydrothermal crystallization with a self-healing effect occurred throughout the whole HA coating layers under an abundant saturated steam environment.

4.2. Bonding strength and failure mechanism

Plasma-sprayed coatings possess inevitable spraying defects which are susceptible to failure, and early failures are often attributed to interfacial failures between the coating and the substrate. For the present study, therefore, the microstructural homogeneity and the bonding strength of a coating to the substrate are concerned in determining the performance and reliability of HACs.

Since the Weibull distribution function can be used to model the reliability and the failure behavior of materials,[18,25,36] a failure rate function $\lambda(\sigma_i)$ shown in Eq. (5) at each corresponding bonding strength is further defined for evaluating the failure mechanism of HACs.

$$\lambda(\sigma_i) = \frac{f(\sigma_i)}{R(\sigma_i)} = \frac{m}{\eta^m}(\sigma_i - \sigma_o)^{m-1} \quad (5)$$

Fig. 8 shows the failure rate function ($\lambda(\sigma)$) and reliability function ($R(\sigma)$) curves of the as-sprayed and hydrothermally treated HACs. These curves start from the minimum strength (σ_o), which implies the failure probability of HACs less than this strength is zero and the reliability of HACs is 1.0. The minimum strength can be recognized as the safety strength for the HACs herein. Meanwhile, knowledge of Weibull modulus (m) can provide further explanation for the self-healing effect of hydrothermal crystallization on the bonding strength of HACs, and it can be used to determine which coating has higher uniformity and reliability. The examination of the Weibull modulus listed in Table 3 represents that HACs are reliable materials with a wear-out failure model ($m > 1$) of increasing failure rate (IFR),[23,36] and HT-HACs in generally show a larger m value compared with the as-sprayed HACs. The Weibull modulus is also a measure of the variability of the data, which being larger as the degree of bonding strength fluctuation decreases. Evident benefits of the cumulative failure probability (Fig. 4(a)) and failure rate (Fig. 8(a)) curves shift to a higher bonding strength with a concentrated data distribution are achieved for HT-HAC specimens. The hydrothermal treatment not only effectively enhances the bonding strength of plasma-sprayed HACs, but helps to acquire more stable HACs with less reliability decrease (Fig. 8(b)) while the loading exceeds the minimum strength.

The representative failure morphologies of these coatings are shown in Fig. 9. According to the criterion of ASTM C633-01, it is recognized that the variation of bonding strength in situ is suggested to be governed by the cohesive strength of coatings and the adhesive strength of a coating to a metal substrate. The cohesive failure (co) is dominated by the microstructural feature such as crystallinity, defects, lamellar texture, and a large area

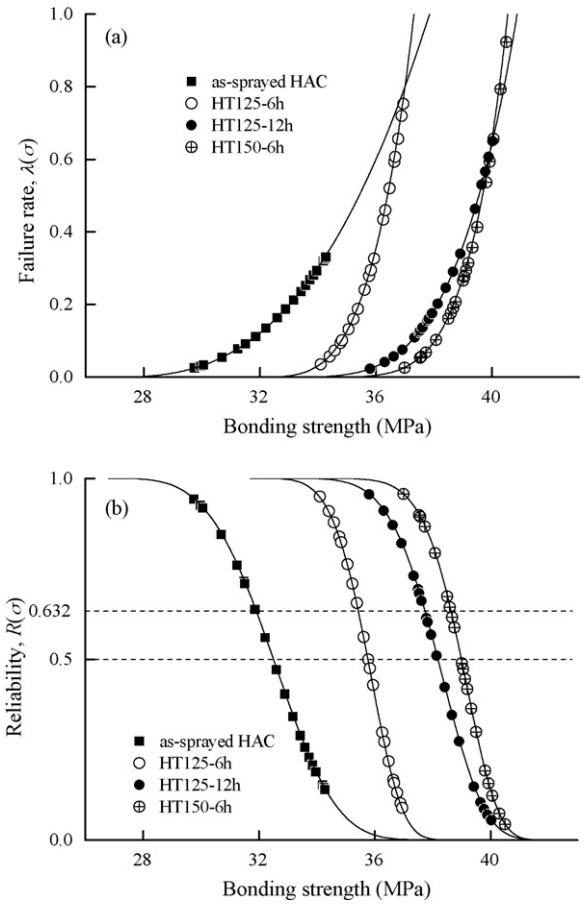

Fig. 8. (a) The failure rate function $\lambda(\sigma)$ curves, and (b) the reliability function $R(\sigma)$ curves of the as-sprayed and various hydrothermally treated HACs. These curves start from the minimum strength (σ_o), which is the safety strength for the biological application of the HACs.

fraction of cohesive failure can be commonly observed at high strength coatings.[9,18] Compared with the failures of as-sprayed HACs shown in Fig. 9(a), since strengthening coatings resulted from the self-healing effect of hydrothermal crystallization, the failure morphologies of HT-HACs represent crystallized, homogeneity and display a larger area fraction of cohesive failure as shown in Fig. 9(b) and (c). In contrast, the decreased area fraction of adhesive failure (ad) represents that the adhesion of HT-HACs to the Ti–6Al–4V substrate is further improved, especially for the HT125-12h specimens. Referring to the evidences demonstrated from the XPS analysis as shown in Fig. 5, the hydrothermal treatment helps to promote the interfacial crystallization through the replenished and the chemisorbed OH^- groups, which results in a significant chemical bonding of the HA coating to Ti–substrate interface.

In our previous study, the better biological responses and lower dissolution rate of HT-HACs with respect to the as-sprayed HACs after 12 weeks of implantation could be attributed to the low contents of amorphous and impurity calcium phosphate phases.[19,33] Furthermore, the improved bonding strength of HT-HACs which resulted from its dense microstructure and enhanced HAC/substrate adhesion is possible to provide better mechanical fixation of the implants without some dissociation

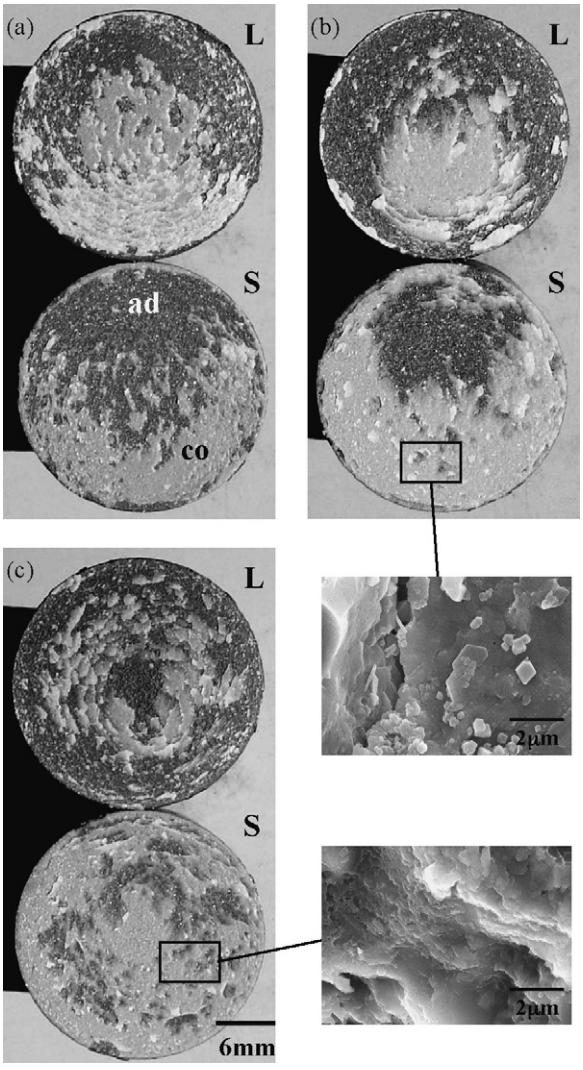

Fig. 9. Failure morphologies of (a) the as-sprayed HACs, (b) HT150-6h, and (c) HT125-12h specimens after tensile adhesion tests. The bonding strength of the coatings measured was a manifestation of cohesive (co) and adhesive (ad) strength (L: loading fixture, S: substrate fixture).

problems. Based on the above-mentioned observations, it can be recognized that the hydrothermal treatment is an available method to improve the mechanical strength, crystallinity, and phase composition of HACs for long-term stable biological and mechanical fixation of implants.

5. Conclusions

The effect of hydrothermal crystallization on the evolution of microstructural features, bonding strength and failure mechanism has been characterized. The results can be summarized as follows:

(1) Hydrothermal crystallization obviously promotes the microstructural homogeneity of plasma-sprayed HACs through the self-healing effect with the grain growth of crystalline HA.
(2) Besides the crystallization effect, the microstructural self-healing significantly further improves the Young's modulus of plasma-sprayed HACs.
(3) XPS analysis results demonstrate that the hydrothermal crystallization modifies the hydroxyl-deficient state of plasma-sprayed HACs with the abundant replenished hydroxyl groups.
(4) The enhanced bonding strength is resulted from the increased cohesive strength of dense coatings and the increased adhesive strength with a significant chemical interlocking between the hydrothermally treated HACs and Ti–substrate interface.
(5) Through the analysis of Weibull distribution function, a wear-out model with an increased Weibull modulus (m) represents that the cohesion, adhesion and the reliability of plasma-sprayed HACs are improved by the hydrothermal crystallization.

Acknowledgments

This study was financially supported by the NCKU Project of Promoting Academic Excellence & Developing World Class Research Centers (No. D96–2700) and the National Science Council of Taiwan (Contract No. NSC 96-2221-E-006-103-MY2) for which we are grateful.

References

1. Munting, E., Verhelpen, M., Li, F. and Vincent, A., Contribution of hydroxy-apatite coatings to implant fixation. In *CRC Handbook of Bioactive Ceramics*, *Vol II*, ed. T. Yamamuro, L. L. Hench and J. Wilson. CRC Press Inc., Boca Raton, FL, 1990, pp. 143–148.
2. Jansen, J. A., van de Waerden, J. P. C. M., Wolke, J. G. C. and de Groot, K., Histologic evaluation of the osseous adaptation to titanium and hydroxyapatite-coated titanium implants. *J. Biomed. Mater. Res.*, 1991, **25**, 973–989.
3. Ogiso, M., TEM analysis of hydroxyapatite-bone interfacial reactions. *J. Dent. Res.*, 1981, **60A**, 419–424.
4. Kitsugi, T., Yamamuro, T., Takeuchi, H. and Ono, M., Bonding behavior of 3 types of hydroxyapatite with different sintering temperatures implanted in bone. *Clin. Orthop.*, 1988, **234**, 280–290.
5. Oonishi, H., Yamamoto, M., Ishimaru, H., Tsuji, E., Kushitani, S., Aono, M. and Ukon, Y., The effect of hydroxyapatite coating on bone growth into porous titanium alloy implants. *J. Bone Joint Surg. B*, 1989, **71**, 213–216.
6. Hardy, D. C. R., Frayssinet, P. and Delince, P. E., Osteointegration of hydroxyapatite-coated stems of femoral prostheses. *Eur. J. Orthop. Surg. Traumatol.*, 1999, **9**, 75–81.
7. Yang, C. Y., Wang, B. C., Chang, E. and Wu, B. C., Bond degradation at the plasma-sprayed HA coating/Ti–6Al–4V alloy interface: an in vitro study. *J. Mater. Sci.: Mater. Med.*, 1995, **6**, 258–265.
8. Wang, B. C., Chang, E., Yang, C. Y., Tu, D. and Tsai, C. H., Characteristics and osteoconductivity of three different plasma-sprayed hydroxyapatite coatings. *Surf. Coat. Technol.*, 1993, **58**, 107–117.
9. Kweh, S. W. K., Khor, K. A. and Cheang, P., Plasma-sprayed hydroxyapatite (HA) coatings with flame-spheroidized feedstock: microstructure and mechanical properties. *Biomaterials*, 2000, **21**, 1223–1234.
10. Sun, L., Berndt, C. C. and Grey, C. P., Phase, structural and microstructural investigations of plasma sprayed hydroxyapatite coatings. *Mater. Sci. Eng.*, 2003, **A360**, 70–84.
11. Gross, K. A., Gross, V. and Berndt, C. C., Thermal analysis of amorphous phases in hydroxyapatite coatings. *J. Am. Ceram. Soc.*, 1998, **81**, 106–112.

12. Feng, C. F., Khor, K. A., Liu, E. J. and Cheang, P., Phase transformations in plasma sprayed hydroxyapatite coatings. *Scripta Mater.*, 2000, **42**, 103–109.
13. Kweh, S. W. K., Khor, K. A. and Cheang, P., High temperature in-situ XRD of plasma sprayed HA coatings. *Biomaterials*, 2002, **23**, 381–387.
14. Lu, Y. P., Song, Y. Z., Zhu, R. F., Li, M. S. and Lei, T. Q., Factors influencing phase compositions and structure of plasma sprayed hydroxyapatite coatings during heat treatment. *Appl. Surf. Sci.*, 2003, **206**, 345–354.
15. Lu, Y. P., Xiao, G. Y., Li, S. T., Sun, R. X. and Li, M. S., Microstructural inhomogeneity in plasma-sprayed hydroxyapatite coatings and effect of post-heat treatment. *Appl. Surf. Sci.*, 2006, **252**, 2142–2421.
16. Li, H., Khor, K. A. and Cheang, P., Properties of heat-treated calcium phosphate coatings deposited by high-velocity oxy-fuel (HVOF) spray. *Biomaterials*, 2002, **23**, 2105–2112.
17. Yang, C. W., Lee, T. M., Lui, T. S. and Chang, E., Effect of post vacuum heating on the microstructural feature and bonding strength of plasma-sprayed hydroxyapatite coatings. *Mater. Sci. Eng.*, 2006, **C26**, 1395–1400.
18. Yang, C. W. and Lui, T. S., Effect of crystallization on the bonding strength and failures of plasma-sprayed hydroxyapatite. *Mater. Trans.*, 2007, **48**, 211–218.
19. Yang, C. W., Lee, T. M., Lui, T. S. and Chang, E., A comparison of the microstructural feature and bonding strength of plasma-sprayed hydroxyapatite coatings with hydrothermal and vacuum post-heat treatment. *Mater. Trans.*, 2005, **46**, 709–715.
20. Yang, Y. C., Chang, E. and Lee, S. Y., Mechanical properties and Young's modulus of plasma-sprayed hydroxyapatite coating on Ti substrate in simulated body fluid. *J. Biomed. Mater. Res.*, 2003, **67A**, 886–899.
21. Tong, W., Chen, J., Cao, Y., Lu, L., Feng, J. and Zhang, X., Effect of water vapor pressure and temperature on the amorphous-to-crystalline HA conversion during heat treatment of HA coatings. *J. Biomed. Mater. Res.*, 1997, **36**, 242–245.
22. Weibull, W., A statistical distribution function of wide applicability. *J. Appl. Mech.*, 1951, **18**, 293–297.
23. Abernethy, R. B., *The New Weibull Handbook: Reliability and Statistical Analysis for Predicting Life, Safety, Survivability, Risk, Cost and Warranty Claims* (*fourth ed.*). North Palm Beach, FL, 2000.
24. Faucher, B. and Tyson, W. R., On the determination of Weibull parameters. *J. Mater. Sci. Lett.*, 1988, **7**, 1199–1203.
25. Burrow, M. F., Thomas, D., Swain, M. V. and Tyas, M. J., Analysis of tensile bond strengths using Weibull statistics. *Biomaterials*, 2004, **25**, 5031–5035.
26. Arias, J. L., Garcia-Sanz, F. J., Mayor, M. B., Chiussi, S., Pou, J., Leon, B. and Perez-Amor, M., Physicochemical properties of calcium phosphate coatings produced by pulsed laser deposition at different water vapour pressures. *Biomaterials*, 1998, **19**, 883–888.
27. Yang, C. W., Lui, T. S. and Chang, E., Low temperature crystallization and structural modification of plasma-sprayed hydroxyapatite coating with hydrothermal treatment. *Adv. Mater. Res.*, 2007, **15–17**, 147–152.
28. Boyd, A., Akay, M. and Meenan, B. J., Influence of target surface degradation on the properties of RF magnetron-sputtered calcium phosphate coatings. *Surf. Interface Anal.*, 2003, **35**, 188–198.
29. Takadama, H., Kim, H. M., Kokubo, T. and Nakamura, T., An X-ray photoelectron spectroscopy study of the process of apatite formation on bioactive titanium metal. *J. Biomed. Mater. Res.*, 2001, **55**, 185–193.
30. Massaro, C., Baker, M. A., Cosentino, F., Ramires, P. A., Klose, S. and Milella, E., Surface and biological evaluation of hydroxyapatite-based coatings on titanium deposited by different techniques. *J. Biomed. Mater. Res.*, 2001, **58B**, 651–657.
31. Healy, K. E. and Ducheyne, P., The mechanisms of passive dissolution of titanium in a model physiological environment. *J. Biomed. Mater. Res.*, 1992, **26**, 319–338.
32. Ramires, P. A., Romito, A. M., Cosentino, F. and Milella, E., The influence of titania/hydroxyapatite composite coatings on *in vitro* osteoblasts behavior. *Biomaterials*, 2001, **22**, 1467–1474.
33. Yang, C. Y., Lee, T. M., Yang, C. W., Chen, L. R., Wu, M. C. and Lui, T. S., The *in vitro* and *in vivo* biological responses of plasma-sprayed hydroxyapatite coatings with post-hydrothermal treatment. *J. Biomed. Mater. Res.*, 2007, **83A**, 263–271.
34. Li, C. J., Ohmori, A. and McPherson, R., The relationship between microstructure and Young's modulus of thermally sprayed ceramic coatings. *J. Mater. Sci.*, 1997, **32**, 997–1004.
35. Kim, H. J. and Kweon, Y. G., Elastic modulus of plasma-sprayed coatings determined by indentation and bend tests. *Thin Solid Films*, 1999, **342**, 201–206.
36. Lima, R. S. and Marple, B. R., High Weibull modulus HVOF titania coatings. *J. Therm. Spray Technol.*, 2003, **12**, 240–249.